Nano World Journal

https://doi.org/10.17756/nwj.2023-s2-065

Research Article

Open Access

Hydrothermal Synthesis and Crystal Structure of a Novel Phosphate: $CdMn_4(HPO_4)_2(PO_4)_2.4H_2O$

Chaymae El Alami, Jamal Khmiyas*, Mohammed Hadouchi, Abderrazzak Assani, Mohamed Saadi and Lahcen El Ammari

Laboratoire de Chimie Appliquée des Matériaux, Centre des Sciences des Matériaux, Faculty of Science, Mohammed V University in Rabat, Avenue Ibn Battouta, BP 1014, Rabat, Morocco

***Correspondence to:**
Jamal Khmiyas
Laboratoire de Chimie Appliquée des Matériaux,
Centre des Sciences des Matériaux,
Faculty of Science,
Mohammed V University in Rabat,
Avenue Ibn Battouta,
BP 1014, Rabat, Morocco.
E-mail: j.khmiyas@um5r.ac.ma

Received: July 25, 2023
Accepted: September 26, 2023
Published: September 29, 2023

Citation: El Alami C, Khmiyas J, Hadouchi M, Assani A, Saadi M, et al. 2023. Hydrothermal Synthesis and Crystal Structure of a Novel Phosphate:$CdMn_4(HPO_4)_2(PO_4)_2.4H_2O$. *NanoWorld J* 9(S2): S383-S388.

Published by United Scientific Group

Abstract

The new cadmium and manganese-based phosphate $CdMn_4(HPO_4)_2(PO_4)_2.4H_2O$, was synthesized by a hydrothermal method and its structure investigated by single crystal X-ray diffraction. The accuracy of the resulting structural model was verified using the Bond-Valence-Sum (BVS) and Charge-Distribution (CD) methods. This phase is a new member of the Hureaulite family and crystallizes within the monoclinic system (space group C2/c, a = 17.6932(5) Å, b = 9.1862(3) Å, c = 9.5417(3) Å, β = 96.562(1)°, and Z = 4). In this crystal structure the metal cations are statically distributed over three independent sites. The first two are located at the general position 8f and are entirely filled by $Cd(1)^{2+}/Mn(1)^{2+}$ and $Cd(3)^{2+}/Mn(3)^{2+}$ while the remaining site is situated at the special position 4e(2) and fully occupied by $Cd(2)^{2+}/Mn(2)^{2+}$. The main structural groups of the asymmetric unit consist of three distorted $[(Cd(1)/Mn(1))O_5(OH_2)]$, $[(Cd(2)/Mn(2))O_6]$, and $[(Cd(3)/Mn(3))O_4(OH_2)_2]$ octahedra with two regular PO_4 and HPO_4 tetrahedra. The 3D-structure is made up of five sequential octahedral $(Cd/Mn)_5O_{16}(OH_2)_6$ units of edge-sharing running along the [001] direction. The connecting PO_4 and HPO_4 groups bind the interconnected units to one another by corners-sharing to create a 3D-framework defining a sizable void along the [001] direction hosting some H_2O molecules.

Keywords

Crystal structure, X-ray diffraction, Hureaulite, Hydrothermal synthesis

Introduction

Over the past decade, much research has been devoted to the conception and design of novel transition metal phosphates [1]. The increased interest in such phases is mostly attributable to their interesting prospective uses, structural variety, and topological diversity [2]. These features are mainly related to the particular chemical behavior of the open mixed frameworks based on metal polyhedra, PO_4^{3-} and HPO_4^{2-} groups. Indeed, the arrangement of such units confers to the crystal structures a high level of thermal, chemical [3] and mechanical stability, creating ideal void spaces that can accommodate cations of different oxidation degrees and sizes [4]. This ability confers attractive physico-chemical properties to phosphate-based materials such electronic, magnetic, optical [5], and electrochemical features [6]. Additionally, hydrated materials belonging to the Hureaulite family are microporous materials and may be used as supplements to create highly corrosion-resistant surfaces and boost steel's wear resistance [7]. In lithiferous pegmatites, Hureaulite is a frequent mineral occurring as a result of the hydrothermal deterioration of triphylite-lithiophilite or another (Fe/Mn) primary phosphate. Hydrothermal processing of Mn-rich phosphate solutions can also yield hureaulite. Hydrothermal synthesis and the treatment under vari-

ous physical and chemical conditions have both been used to create simple and mixed hureaulite crystals. In other works, Hureaulite crystals were obtained at ambient temperature and pressure by a reflux procedure [8]. In connection with our systematic hydrothermal studies of metal orthophosphates, we have previously synthesized and characterized a number of compounds with various 3D-networks viz. $M_2Mn_3(HPO_4)_2(PO_4)_2$ (M = Pb, Sr) (Monoclinic system, space group $P2_1/c$ and Z = 2) [9, 10], γ-$AgZnPO_4$ belonging to ABW zeolite family (Monoclinic system, space group $P2_1/n$ and Z = 4) [11], $Ag_2Co_3(HPO_4)(PO_4)_2$ (Orthorhombic system, space group *Ima2* and Z = 4) [12] that crystalize in α-$CrPO_4$ structure-type, $AgMg_3(HPO_4)_2(PO_4)$ member of the well-known alluaudite group (Monoclinic system, space group *C2/c* and Z = 2) [13]. Other phosphates that are the first representatives of their series like $AgSr_4Cu_{4.5}(PO_4)_6$ (Triclinic system, space group *P-1* and Z = 2) [14], and $SrFe(HPO_4)(PO_4)$ (Triclinic system, space group *P-1* and Z = 2) [15] were likewise isolated. Moreover, a special focus was devoted to the systematic study of CdO-MnO-P_2O_5-H_2O resulting in the elaboration of the new phosphate $CdMn_4HOP_4)_2(PO_4)_2.4H_2O$ with a Hureaulite-like structure. The crystal structure of this phosphate was determined through single crystal X-ray diffraction and its structural model's correctness was verified using the BVS [16] approach and CD evaluation [17].

Experimentation

Synthesis

Single crystals of the novel compound $CdMn_4HOP_4)_2(PO_4)_2.4H_2O$ were grown hydrothermally with the appropriate reaction mixture of Mn, $CdCl_2$, and H_3PO_4 (85% by weight) according to the molar ratio Mn:Cd:P = 3:2:4. The process was carried out under autogenous pressure at 468 K for 3 days in an appropriate autoclave reactor with PTFE lined vessel (23 ml) filled with 12 ml of deionized water. The resulting product was filtered, rinsed with deionized water, and dried at room temperature. The structure is determined at nanometric scale.

Results and Discussion

Structure determination

Adequate single crystal was fixed by a small diameter glass fibre to a Bruker X8 APEXII diffractometer for the collection of X-ray diffraction data. The gathering of intensities was performed by means of the X-ray Mokα radiation (λ_{Mo} = 0.71073 Å) via the φ and ω scanning modes. Acquired intensities were afterwards corrected for Lorentz and polarization effects by means of SAINT program [18]. Additionally, further absorption corrections were carried out using SADABS program [19] and resulted in a total of 20791 intensities of which 5338 are independent and 4587 with I > 2σ(I) requirement. Based on these crystal data, the structural determination of this new phosphate was performed via WinGX package [20]. The crystal structure was solved by Direct Methods with SHELXT 2014/7 program [21] and refined by full-matrix least-squares using SHELXL2018/3 [22] program. As a result of structural resolution Cd, Mn, and P atoms were located initially. After several successive refinement and Fourier-difference analysis, the remaining oxygen and hydrogen atoms were positioned with d_{O-H} = 0.82Å to fulfill the asymmetric unit. In this crystal structure, the position of the hydrogen atoms has been refined isotropically by adopting a riding model with $U_{iso}(H)$ = 1.5 $U_{eq}(O)$. During the last refinement cycle, the lowest and highest residual electron densities are $\Delta\rho_{min}$ = -0.64 e.Å^{-3} at 0.43 Å from P1 and $\Delta\rho_{max}$ = 0.66 e.Å^{-3} locating at 0.64Å from Mn1. Crystallographic features, data gathering details and structure refinement results are listed in table 1.

Table 1: Crystallographic data, X-ray collection details and structure refinement results for $CdMn_4(HPO_4)_2(PO_4)_2.4H_2O$.

Crystallographic details	
Chemical formula	$CdMn_4(HPO_4)_2(PO_4)_2.4H_2O$
M_r	786.12
System, space group	Monoclinic, *C2/c*
T (K)	296
a, *b*, *c* (Å)	17.6932 (5), 9.1862 (3), 9.5417 (3)
β (°)	96.562 (1)
V (Å^3)	1540.68 (8)
Z	4
Mo Kα	λ = 0.71073 Å
μ (mm^{-1})	5.08
Data gathering	
θ_{min}, θ_{max} (°)	3.2, 42.3
Miller indices	-33 ≤ h ≤ 29, -17 ≤ k ≤ 13, -16 ≤ l ≤ 17
Measured reflections	20791
Independent reflections	5338
Reflections with $I > 2\sigma(I)$	4587
R_{int}	0.029
$(\sin\theta/\lambda)_{max}$ (Å^{-1})	0.947
Refinement	
$R[F^2 > 2s(F^2)]$, $wR(F^2)$, *S*	0.022, 0.050, 1.03
Number of parameters	139
$\Delta\rho_{max/min}$ (e Å^{-3})	0.66, -0.64

Elemental coordinates and their respective displacement parameters are reported in table 2. Selection of inter-atomic bond lengths and angles are given in table 3 and geometrical features of hydrogen bond are listed in table 4. All representations were done by means of Vesta-3 [23].

Structural description

The principal building groups of the asymmetric unit in the crystal structure of $CdMn_4(HPO_4)_2(PO_4)_2.4H_2O$ are three distorted [(Cd(1)/Mn(1))$O_5(OH_2)$], [(Cd(2)/Mn(2))O_6], and [(Cd(3)/Mn(3))$O_4(OH_2)_2$] octahedra with two regular PO_4^{3-}/HPO_4^{2-} tetrahedra. The 3D-framework results from $(Cd/Mn)_5O_{16}(OH_2)_6$ octahedral pentameric entities of edge-sharing running along the [100] direction (Figure 1). Neighboring entities are interconnected by corner-sharing [(Cd(1)/Mn(1))$O_5(OH_2)$] - [(Cd(3)/Mn(3))$O_4(OH_2)_2$] and bridged by apical PO_4^{3-} and HPO_4^{2-} units. Such polyhedral arrangement generates a large cavities extending parallel to the [001] direction that accommodates terminal H_2O molecules of [Cd(3)/Mn(3))$O_4(OH_2)_2$] groups (Figure 2). Additional interstitial Hydrogen interaction O—H···O contributes to the cohesion of the crystal structure. The geometrical

Table 2: Atomic positions and isotropic or equivalent thermal parameters (Å²) in $CdMn_4(HPO_4)_2(PO_4)_2.4H_2O$.

Atom	Site	x	y	z	U_{iso}*/U_{eq}	Occ. (< 1)
Cd1	8f	0.17489 (2)	1.02882 (2)	0.86620 (2)	0.00913 (3)	0.395 (2)
Mn1	8f	0.17489 (2)	1.02882 (2)	0.86620 (2)	0.00913 (3)	0.606 (2)
Cd2	4e	0.000000	1.10366 (2)	1.250000	0.00881 (5)	0.095 (2)
Mn2	4e	0.000000	1.10366 (2)	1.250000	0.00881 (5)	0.905 (2)
Mn3	8f	0.31910 (2)	0.91115 (2)	0.68516 (2)	0.00964 (4)	0.942 (2)
Cd3	8f	0.31910 (2)	0.91115 (2)	0.68516 (2)	0.00964 (4)	0.056 (2)
P1	8f	0.16055 (2)	0.73824 (3)	0.62771 (3)	0.00652 (5)	
P2	8f	0.08232 (2)	0.82066 (3)	1.08928 (3)	0.00721 (5)	
O1	8f	0.07628 (4)	0.73412 (8)	0.65777 (8)	0.0104 (2)	
O2	8f	0.16333 (4)	0.76055 (9)	0.46742 (8)	0.0109 (2)	
O3	8f	0.20089 (4)	0.59525 (8)	0.67326 (8)	0.0114 (2)	
O4	8f	0.20237 (4)	0.86518 (9)	0.70852 (8)	0.0115 (2)	
O5	8f	0.08362 (4)	0.88993 (9)	0.94412 (8)	0.0127 (2)	
O6	8f	0.01192 (5)	0.7156 (2)	1.08075 (9)	0.0157 (2)	
H6	8f	-0.0170 (9)	0.726 (2)	1.008 (2)	0.036 (6)*	
O7	8f	0.15367 (4)	0.72971 (9)	1.13261 (8)	0.0125 (2)	
O8	8f	0.07625 (4)	0.93321 (9)	1.20408 (8)	0.0129 (2)	
O9	8f	0.26100 (5)	1.08249 (9)	0.53182 (8)	0.0127 (2)	
H9A	8f	0.241933	1.147159	0.575491	0.019*	
H9B	8f	0.287807	1.133976	0.487601	0.019*	
O10	8f	0.42335 (5)	1.0122 (2)	0.6521 (2)	0.0208 (2)	
H10A	8f	0.435067	1.078223	0.708092	0.031*	
H10B	8f	0.462555	0.970597	0.636459	0.031*	

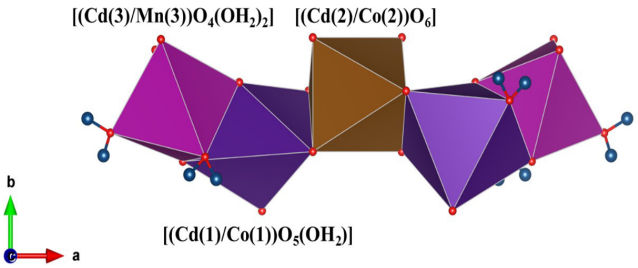

Figure 1: Edge-sharing $[(Cd(1)/Mn(1))O_5(OH_2)]$, $[(Cd(2)/Mn(2))O_6]$, and $[(Cd(3)/Mn(3))O_4(OH_2)_2]$ octahedra building a pentameric entity parallel to the [100] direction.

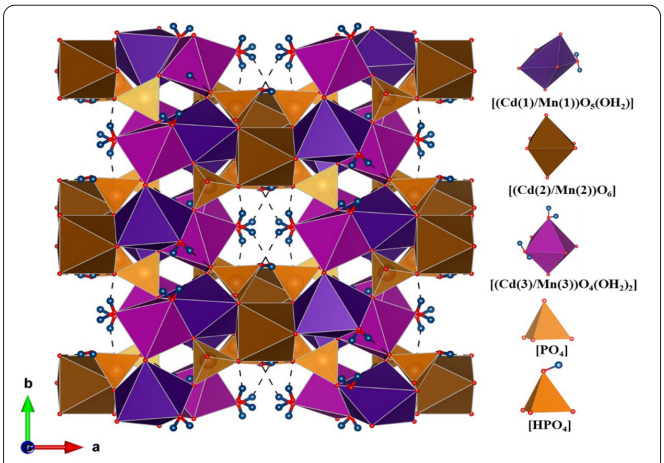

Figure 2: Perspective view of $CdMn_4(HPO_4)_2(PO_4)_2.4H_2O$ crystal structure along the c-axis revealing hydrogen bonding (dashed lines).

characteristics of those O-H..O are entirely in line with those described in the literature, particularly $M_2Mn_3(HPO_4)_2(PO_4)_2$ (M = Pb, Sr) [9, 10].

Structural investigation

The accuracy and stability of the given structural model was assessed herein by means of the BVS and CD analytical approaches. The electrical charge distribution calculations were performed with the CHARDI2015 program [24], while the BVS values were obtained with the EXPO2014 program [25] (Table 5).

Considering the present structural model all constituent elements of the asymmetric unit are in general positions (Wyckoff position 8f) except (Cd2/Mn2) that are positioned on 4e position. Distribution of the positively charged elements on the first ten independent crystallographic sites reveals that the cations (Cd^{2+}/Mn^{2+}), P^{5+}, and H^{+} occupy fully their respective positions. The calculated charge values Q(j) corresponding to the various cations are in complete accordance with their respective C(j).SO(j) values. This result is also supported by the charge ratios C(j)/Q(j) ≈ 1 in all cases and the smaller divergence of Q(i) from C(j) which is corroborated by the absolute mean (MAPD = 7.8%). A close comparison between the computed cationic V(j), compared to their formal valences, reveals that the BVS calculations lead to the expected results with an interesting global instability index (GII) of 0.092 v.u. In the structure of this Cd/Mn-Hureaulite half of the crystallographic sites are occupied by cations. The first three are mutually filled by Cd1/Mn1, Cd2/Mn2, and Cd3/Mn3 with occupancy rates of 0.395(2)/0.606(2), 0.095(2)/0.905(2), and 0.942(2)/0.056(2), respectively. These mixed sites are closely bounded to six adjacent O atoms resulting in more or less deformed octahedra with significant traction stress (Under bonding effect). In this asymmetric unit both P atoms are ar-

Table 3: Main bond lengths and angles in $CdMn_4(HPO_4)_2(PO_4)_2.4H_2O$.

Bond	Length (Å)	Bond	Length (Å)
Cd1/Mn1—O2	2.1826 (8)	Cd3/Mn3—O10	2.1205 (9)
Cd1/Mn1 —O4	2.2197 (8)	Cd3/Mn3—O4	2.1446 (8)
Cd1/Mn1—O8	2.2234 (8)	Cd3/Mn3—O7	2.1768 (8)
Cd1/Mn1—O5	2.2500 (8)	Cd3/Mn3—O2	2.1926 (8)
Cd1/Mn1—O9	2.3051 (8)	**< Cd3/Mn3—O> = 2.1935 Å**	
Cd1/Mn1—O3	2.3524 (8)	P1—O3	1.5339 (8)
< Cd1/Mn1—O> = 2.2555 Å		P1—O4	1.5399 (8)
Cd2/Mn2—O8	2.1445 (8)	P1—O2	1.5494 (8)
Cd2/Mn2—O8	2.1445 (8)	P1—O1	1.5507 (8)
Cd2/Mn2—O5	2.2354 (8)	**< P1—O> = 1.5435 Å**	
Cd2/Mn2—O5	2.2354 (8)	P2—O8	1.5190 (8)
Cd2/Mn2—O1	2.2557 (8)	P2—O5	1.5268 (8)
Cd2/Mn2—O1	2.2557 (8)	P2—O7	1.5307 (8)
< Cd2/Mn2—O> = 2.2118 Å		P2—O6	1.5706 (8)
Cd3/Mn3—O3	2.2180 (8)	**< P2—O> = 1.5368 Å**	
Cd3/Mn3—O9	2.3090 (8)		
Bond	**Angles (°)**	**Bond**	**Angles (°)**
O2—Cd1/Mn1—O8	93.61 (3)	O8—Cd1/Mn1—O9	162.05 (3)
O4—Cd1/Mn1—O8	81.37 (3)	O5—Cd1/Mn1—O9	87.99 (3)
O2—Cd1/Mn1—O5	104.44 (3)	O2—Cd1/Mn1—O3	88.70 (3)
O4—Cd1/Mn1—O5	93.50 (3)	O4—Cd1/Mn1—O3	77.65 (3)
O8—Cd1/Mn1—O5	77.46 (3)	O8—Cd1/Mn1—O3	121.43 (3)
O2—Cd1/Mn1—O9	100.25 (3)	O9—Cd1/Mn1—O3	70.64 (3)
O4—Cd1/Mn1—O9	89.17 (3)		
O8—Cd2/Mn2—O8	86.20 (5)	O5—Cd2/Mn2—O1	86.39 (3)
O8—Cd2/Mn2—O5	79.41 (3)	O5—Cd2/Mn2—O1	91.62 (3)
O8—Cd2/Mn2—O5	102.84 (3)	O8—Cd2/Mn2—O1	89.10 (3)
O8—Cd2/Mn2—O5	102.84 (3)	O5—Cd2/Mn2—O1	91.62 (3)
O8—Cd2/Mn2—O5	79.41 (3)	O5—Cd2/Mn2—O1	86.39 (3)
O5—Cd2/Mn2—O5	176.98 (5)	O1—Cd2/Mn2—O1	97.30 (4)
O8—Cd2/Mn2—O1	89.10 (3)		
O10—Mn3—O7	105.21 (4)	O4—Mn3—O9	80.54 (3)
O4—Mn3—O7	85.86 (3)	O2—Mn3—O9	98.99 (3)
O10—Mn3—O3	87.66 (3)	O3—Mn3—O9	77.04 (3)
O4—Mn3—O3	82.20 (3)	O10—Mn3—O2	91.37 (3)
O7—Mn3—O3	90.17 (3)	O4—Mn3—O2	97.97 (3)
O2—Mn3—O3	175.96 (3)	O7—Mn3—O2	93.87 (3)
O10—Mn3—O9	86.51 (4)		
O3—P1—O4	108.98 (5)	O3—P1—O1	110.66 (4)
O3—P1—O2	109.07 (4)	O4—P1—O1	110.06 (4)
O4—P1—O2	109.05 (4)	O2—P1—O1	108.99 (4)
O8—P2—O5	112.34 (5)	O8—P2—O6	109.55 (5)
O8—P2—O7	107.51 (5)	O5—P2—O6	107.65 (4)
O5—P2—O7	112.03 (5)	O7—P2—O6	107.66 (5)

Table 4: Hydrogen-bond geometry (Å, °) in $CdMn_4(HPO_4)_2(PO_4)_2.4H_2O$ structure.

D—H···*A*	*D*—H	H···*A*	*D*···*A*	*D*—H···*A*
O6—H6···O1	0.82 (1)	1.80 (1)	2.6137 (11)	175 (2)
O6—H6···O2	0.82 (1)	2.65 (2)	3.1097 (12)	117 (2)
O9—H9*A*···O7	0.82	2.05	2.8150 (12)	155
O9—H9*B*···O7	0.82	1.85	2.6668 (11)	172
O10—H10*B*···O6	0.82	2.02	2.7455 (13)	147
O10—H10*A*···O1	0.82	1.95	2.7294 (13)	160

ranged in a conventional tetrahedral environment, with the coordination ratios ECoN (P1)/CN(P1) = 4/4 and ECoN (P2)/CN(P2) = 3.98/4. The monovalent cations H^+6, H^+9A, H^+9B, H^+10A, and H^+10B which are implied in weak hydrogen bonding exhibit suitable results of ECoN(H6) = 1.33, ECoN(H9A) = 1.16, ECoN(H9B) = 1.29, ECoN(H10A) = 1.17, and ECoN(H10B) = 1.22 [26].

Conclusion

Single crystals of the novel phase $CdMn_4(HPO_4)_2(PO_4)_2.4H_2O$ have been elaborated under mild hydrothermal conditions and characterized by single-crystal X-ray diffraction. The correctness of the resulting structural model was confirmed by means of BVS and CD methods. According to the current structural model, all atoms of the asymmetric unit are in general positions (Wyckoff position 8f), with the exception of Cd2/Mn2, which is in 4e position. The cationic charge distribution on the first

Table 5: Cationic BVS and CD results in $CdMn_4(HPO_4)_2(PO_4)_2.4H_2O$.

Ion	C(j).SO(j)	N(j)	ECoN(j)	V(j)	Q(j)	C(j)/Q(i)
Cd(1)/Mn(1)	2	6	5.86	1.87	1.87	1.07
Cd(2)/Mn(2)	2	6	5.90	1.84	1.78	1.13
Cd(3)/Mn(3)	2	6	5.84	1.90	1.99	1.00
P(1)	5	4	4	4.88	5.14	0.97
P(2)	5	4	3.98	4.98	4.7	1.05
H6	1	1	1.33	1.17	0.99	1.01
H9A	1	1	1.16	1.10	0.86	1.17
H9B	1	1	1.29	1.02	0.87	1.15
H10A	1	1	1.17	0.98	0.88	1.13
H10B	1	1	1.22	1.00	0.89	1.13

Note: C(j) = oxidation state; N(j) = classical coordination number; SO(j) = site occupancy factor V(j) = computed valence; Q(i) = computed charge; and ECoN(j) = effective coordination number.

ten independent crystallographic sites reveals that (Cd^{2+}/Mn^{2+}), P^{5+}, and H^+ fully occupy their sites. In addition, the calculated charge values Q(j) assigned to the various cations are in perfect agreement with the weighted values C(j).SO(j). This finding is confirmed by charge ratios C(j)/Q(j) ≈ 1 in all cases, as well as the lowest divergence of Q(i) from C(j), which is supported by the absolute mean (MAPD = 7.8%). A comprehensive examination of the computed cationic valences V(j) and their formal charges indicates that the BVS calculations provide the expected results, with an interesting GII of 0.092 v.u. The 3D-net framework results from $(Cd/Mn)_5O_{16}(OH_2)_6$ octahedral pentameric entities of edge-sharing extending along the [100] direction. Adjacent entities are linked to each other by corner-sharing [(Cd(1)/Mn(1))$O_5(OH_2)$], [(Cd(3)/Mn(3))$O_4(OH_2)_2$], PO_4^{3-}, and HPO_4^{2-}. This polyhedral disposition creates sizable cavities parallel to the [001] direction which contain the terminal H_2O molecules of the [(Cd(3)/Mn(3))$O_4(OH_2)_2$] polyhedra. The cohesiveness of the crystal structure is enhanced by additional O—H…O interstitial H-interactions.

Acknowledgements

The authors would like to thank the (UATRS, CNRST) Rabat, Morocco for their contribution to the X-ray analysis.

Conflict of Interest

None.

Funding

This work was fully funded by Mohammed V University, Rabat, Morocco.

References

1. Rao CNR, Natarajan S, Neeraj S. 2000. Building open-framework metal phosphates from amine phosphates and a monomeric four-membered ring phosphate. *J Solid State Chem* 152(1): 302-321. https://doi.org/10.1006/jssc.2000.8676
2. Khmiyas J, Assani A, Saadi M, El Ammari L. 2016. Synthesis and crystal structure of calcium dizinc iron(III) tris(orthophosphate), $CaZn_2Fe(PO_4)_3$. *Acta Cryst Sec E Cryst Commun* 72(9): 1260-1262. https://doi.org/10.1107/S2056989016012421
3. Morozov VA, Pokholok KV, Lazoryak BI, Malakho AP, Lachgar A, et al. 2003. A new iron oxophosphate $SrFe_3(PO_4)_3O$ with chain-like structure. *J Solid State Chem* 170(2): 411-417. https://doi.org/10.1016/S0022-4596(02)00133-0
4. Zhao H, Yuan ZY. 2020. Insights into transition metal phosphate materials for efficient electrocatalysis. *Chem Cat Chem* 12(15): 3797-3810. https://doi.org/10.1002/cctc.202000360
5. Zaghib K, Mauger A, Goodenough JB, Gendron F, Julien CM. 2007. Electronic, optical, and magnetic properties of $LiFePO_4$: small magnetic polaron effects. *Chem Mater* 19(15): 3740-3747. https://doi.org/10.1021/cm0710296
6. Shi Q, Zhang L, Schlesinger ME, Boerio-Goates J, Woodfield BF. 2013. Low temperature heat capacity study of $FePO_4$ and $Fe_3(P_2O_7)_2$. *J Chem Thermodyn* 62: 35-42. https://doi.org/10.1016/j.jct.2013.02.017
7. Yin H, Liu F, Chen X, Feng X, Tan W, et al. 2012. Synthesis of hureaulite by a reflux process at ambient temperature and pressure. *Microporous Mesoporous Mater* 153: 115-123. https://doi.org/10.1016/j.micromeso.2011.11.057
8. Frost RL, Xi Y, Scholz R, López A, Belotti FM. 2013. Vibrational spectroscopic characterization of the phosphate mineral hureaulite–$(Mn, Fe)_5(PO_4)_2(HPO_4)_2.4(H_2O)$. *Vibr Spectrosc* 66: 69-75. https://doi.org/10.1016/j.vibspec.2013.02.003
9. Khmiyas J, Assani A, Saadi M, El Ammari L. 2013. Distrontium trimanganese(II) bis(hydrogenphosphate) bis(orthophosphate). *Acta Cryst Sec E Cryst Commun* 69(8): i50. https://doi.org/10.1107/S1600536813018898
10. Assani A, Saadi M, Zriouil M, El Ammari L. 2012. Dilead(II) trimanganese(II) bis(hydrogenphosphate) bis(phosphate). *Acta Cryst Sec E Cryst Commun* 68(8): i66. https://doi.org/10.1107/S1600536812033259
11. Assani A, Saadi M, El Ammari L. 2010. The γ-polymorph of $AgZnPO_4$ with an ABW zeolite-type framework topology. *Acta Cryst Sec E Cryst Commun* 66(11): i74. https://doi.org/10.1107/S1600536810038717
12. Assani A, El Ammari L, Zriouil M, Saadi M. 2011. Disilver(I) tricobalt(II) hydrogenphosphate bis(phosphate), $Ag_2Co_3(HPO_4)(PO_4)_2$. *Acta Cryst Sec E Cryst Commun* 67(7): i41. https://doi.org/10.1107/S1600536811022598
13. Assani A, Saadi M, Zriouil M, El Ammari L. 2011. Silver trimagnesium phosphate bis(hydrogenphosphate), $AgMg_3(PO_4)(HPO_4)_2$, with an alluaudite-like structure. *Acta Cryst Sec E Cryst Commun* 67(1): i5. https://doi.org/10.1107/S1600536810053304
14. Khmiyas J, Benhsina E, Ouaatta S, Assani A, Saadi M, et al. 2020. Crystal structure of silver strontium copper orthophosphate, $AgSr_4Cu_{4.5}(PO_4)_6$. *Acta Cryst Sec E Cryst Commun* 76(2): 186-191. https://doi.org/10.1107/S2056989020000109
15. Khmiyas J, Assani A, Saadi M, El Ammari L. 2022. Crystal structure, charge-distribution and bond-valence-sum investigations of a new

layered phosphate $SrFe(HPO_4)(PO_4)$. *Mater Today Proc* 58: 994-998. https://doi.org/10.1016/j.matpr.2021.12.458

16. Altermatt D, Brown ID. 1985. The automatic searching for chemical bonds in inorganic crystal structures. *Acta Cryst Sec B Struct Sci Cryst Eng Mater* 41(4): 240-244. https://doi.org/10.1107/S0108768185002051
17. Nespolo M. 2016. Charge distribution as a tool to investigate structural details. IV. A new route to heteroligand polyhedra. *Acta Cryst Sec B Struct Sci Cryst Eng Mater* 72(1): 51-66. https://doi.org/10.1107/S2052520615019472
18. Bruker SAINT. 2012. Bruker AXS Inc., Madison, Wisconsin, USA.
19. Krause L, Herbst-Irmer R, Sheldrick GM, Stalke D. 2015. Comparison of silver and molybdenum microfocus X-ray sources for single-crystal structure determination. *J Appl Cryst* 48(1): 3-10. https://doi.org/10.1107/S1600576714022985
20. Farrugia LJ. 2012. WinGX and ORTEP for Windows: an update. *J Appl Cryst* 45(4): 849-854. https://doi.org/10.1107/S0021889812029111
21. Sheldrick GM. 2015. SHELXT-Integrated space-group and crystal-structure determination. *Acta Cryst Sec A Found Adv* 71(1): 3-8. https://doi.org/10.1107/S2053273314026370
22. Sheldrick GM. 2015. Crystal structure refinement with SHELXL. *Acta Cryst Sec C Struct Chem* 71(1): 3-8. https://doi.org/10.1107/S2053229614024218
23. Momma K, Izumi F. 2011. VESTA 3 for three-dimensional visualization of crystal, volumetric and morphology data. *J Appl Cryst* 44(6): 1272-1276. https://doi.org/10.1107/S0021889811038970
24. Nespolo M, Guillot B. 2016. CHARDI2015: charge distribution analysis of non-molecular structures. *J Appl Cryst* 49(1): 317-321. https://doi.org/10.1107/S1600576715024814
25. Altomare A, Cuocci C, Giacovazzo C, Moliterni A, Rizzi R, et al. 2013. EXPO2013: a kit of tools for phasing crystal structures from powder data. *J Appl Cryst* 46(4): 1231-1235. https://doi.org/10.1107/S0021889813013113
26. Nespolo M, Ferraris G, Ivaldi G, Hoppe R. 2001. Charge distribution as a tool to investigate structural details. II. Extension to hydrogen bonds, distorted and hetero-ligand polyhedra. *Acta Cryst Sec B Struct Sci* 57(5): 652-664. https://doi.org/10.1107/S0108768101009879